Nuclear matrix elements of neutrinoless double-β decay in the triaxial projected shell model

Y. K. Wang [●],[1] P. W. Zhao,[1] and J. Meng [●][1,2,*]

[1]*State Key Laboratory of Nuclear Physics and Technology, School of Physics, Peking University, Beijing 100871, China*
[2]*Yukawa Institute for Theoretical Physics, Kyoto University, Kyoto 606-8502, Japan*

The nuclear matrix elements of neutrinoless double-β decay for nuclei ^{76}Ge, ^{82}Se, ^{100}Mo, ^{130}Te, and ^{150}Nd are studied within the triaxial projected shell model, which incorporates simultaneously the triaxial deformation and quasiparticle configuration mixing. The low-lying spectra, the $B(E2 : 0^+ \rightarrow 2^+)$ values, and the occupancies of single-particle orbits are reproduced well. The effects of the quasiparticles configuration mixing, the triaxial deformation, and the closure approximation on the nuclear matrix elements are studied in detail. For nuclei ^{76}Ge, ^{82}Se, ^{100}Mo, ^{130}Te, and ^{150}Nd, the nuclear matrix elements are respectively reduced by the quasiparticle configuration mixing by 6%, 7%, 2%, 3%, and 4%, and enhanced by calculating explicitly the transitions through odd-odd intermediate states by 7%, 4%, 11%, 20%, and 14%. Varying the triaxial deformation γ from 0° to 60° for the mother and daughter nuclei, the nuclear matrix elements change by 41%, 17%, 68%, 14%, and 511%, respectively, for ^{76}Ge, ^{82}Se, ^{100}Mo, ^{130}Te, and ^{150}Nd, which indicates the importance of treating the triaxial deformation consistently in calculating the nuclear matrix elements.

I. INTRODUCTION

The neutrinoless double-β^- ($0\nu\beta\beta$) decay is a nuclear weak process in which an even-even nucleus (N, Z) decays to its even-even neighbor $(N - 2, Z + 2)$ by emitting only two electrons. It is a lepton-number-violating process and provides a sensitive probe to explore the Majorana nature of the neutrino [1]. The $0\nu\beta\beta$ decay is also regarded as an effective tool to determine the hierarchy of the neutrino mass spectrum [2,3]. Due to its great importance in revealing information associated with the fundamental physics, the detection of $0\nu\beta\beta$ decay has become the goal of several experimental projects worldwide [4–11].

In the light-neutrino exchange mechanism, the half-life $T_{1/2}^{0\nu}$ of the $0\nu\beta\beta$ decay connects directly with the effective neutrino mass [12],

$$\left[T_{1/2}^{0\nu}\right]^{-1} = G_{0\nu} g_A^4(0) \left| \frac{\langle m_{\beta\beta} \rangle}{m_e} \right|^2 |M^{0\nu}|^2. \qquad (1)$$

Here, m_e is the electron mass, $\langle m_{\beta\beta} \rangle$ is the effective neutrino mass, $g_A(0)$ is the axial-vector coupling constant, and $G_{0\nu}$ is the kinematic phase-space factor [13]. Obviously, the accurate determination of the nuclear matrix element (NME) $M^{0\nu}$ is crucial for extracting the $\langle m_{\beta\beta} \rangle$ from the experimental half-life.

The NME $M^{0\nu}$ depends on the decay operator and the nuclear many-body wave functions. The decay operator is derived from the second-order weak Hamiltonian constructed by the charged nucleonic and leptonic currents [14]. The effects from the higher-order terms and the two-body currents on the

decay operator have been studied extensively [15–18], and the quality of nonrelativistic reduction of the decay operator is also examined within a fully relativistic framework [14,19]. The nuclear many-body wave functions are obtained from various nuclear models, including the configuration interaction shell model (SM) [20–23], the quasiparticle random-phase approximation (QRPA) [24–27], the interacting boson model (IBM) [28,29], the projected Hartree-Fock-Bogoliubov model (PHFB) [30–32], and the generator coordinate method (GCM) based on the relativistic [19,33,34] and nonrelativistic [35,36] density-functional theories (DFTs), etc. These models are restricted either by the model space or the many-body correlations, which leads to the fact that the predicted NMEs differ by a factor two to three [3].

The triaxial projected shell model (TPSM) carries out the configuration mixing based on a Nilsson mean field with the angular-momentum projection technique [37]. It has been successfully applied to study the nuclear rotational excitations, including the backbending phenomena [38], the superdeformed rotational bands [39], the signature inversion [40], the γ bands [41], and the chiral [42–44] and wobbling [45] rotations.

The simplified version of TPSM, namely the PHFB in axial deformation case, is performed to study the NMEs of $0\nu\beta\beta$ decay [30–32]. With the help of the Pfaffian algorithm [46,47] to evaluate the matrix elements of many-body operators, the newly developed TPSM in Refs. [42,44] include triaxial deformation and the configuration interaction induced by the quasiparticle excitations beyond the HFB vacuum, and treat even-even and the odd-odd nuclear systems simultaneously. This provides us an opportunity to study the effects of the triaxial deformation and quasiparticle configuration mixing, and the effects beyond the closure approximation on the NMEs.

*mengj@pku.edu.cn

In this paper, the TPSM is applied to investigate the NMEs of $0\nu\beta\beta$ decay for nuclei ^{76}Ge, ^{82}Se, ^{100}Mo, ^{130}Te, and ^{150}Nd. The influence of the triaxial deformation, the quasiparticles configuration mixing, and the commonly used closure approximation will be examined.

II. THEORETICAL FRAMEWORK

A. Decay operator

The charged-current weak Hamiltonian for the $0\nu\beta\beta$ decay is [48]

$$\mathcal{H}_{\text{weak}}(x) = \frac{G_F \cos\theta_C}{\sqrt{2}} j^\mu(x)\mathcal{J}_\mu^\dagger(x) + \text{H.c.}, \tag{2}$$

where G_F and θ_C are the Fermi constant and Cabbibo angle, respectively. The standard leptonic current j^μ is

$$j^\mu = \bar{e}(x)\gamma^\mu(1 - \gamma_5)\nu_e(x), \tag{3}$$

and the hadronic current is expressed in terms of nucleon field ψ as

$$\mathcal{J}_\mu^\dagger = \bar{\psi}(x)\left[g_V(q^2)\gamma_\mu + ig_M(q^2)\frac{\sigma_{\mu\nu}}{2m_p}q^\nu - g_A(q^2)\gamma_\mu\gamma_5 - g_P(q^2)q_\mu\gamma_5\right]\tau_-\psi(x). \tag{4}$$

Here, m_p is the nucleon mass, q^μ is the transferred momentum from hadrons to leptons, the isospin lowering operator $\tau_- \equiv (\tau_1 - i\tau_2)/2$, and $\sigma_{\mu\nu} \equiv i/2[\gamma_\mu, \gamma_\nu]$. The momentum-dependent form factors $g_V(q^2)$, $g_M(q^2)$, $g_A(q^2)$, and $g_P(q^2)$ incorporate the correction of the finite nucleon size and are reduced to the vector, weak-magnetism, axial-vector, and induced pseudoscalar coupling constants, respectively, in the zero-momentum-transfer limit. The detailed formulas of the form factors can be found in Ref. [15].

Assuming that $0\nu\beta\beta$ decay is mediated by the light Majorana neutrinos, adopting the long-wave approximation for the outgoing electrons, and neglecting the small energy transferred between nucleons, the NME can be derived with the help of the S matrix in the framework of second-order perturbative theory [19],

$$M^{0\nu} = \langle\Psi_D|\hat{\mathcal{O}}^{0\nu}|\Psi_M\rangle. \tag{5}$$

Here, $|\Psi_M\rangle$ and $|\Psi_D\rangle$ are respectively the nuclear wave functions of the mother and daughter nuclei, and the decay operator $\hat{\mathcal{O}}^{0\nu}$ reads

$$\hat{\mathcal{O}}^{0\nu} = \frac{4\pi R}{g_A^2(0)}\iint d^3x_1 d^3x_2 \int \frac{d^3q}{(2\pi)^3}\frac{e^{iq\cdot(x_1-x_2)}}{|q|}\sum_m \frac{\mathcal{J}_\mu^\dagger(x_1)|m\rangle\langle m|\mathcal{J}^{\mu\dagger}(x_2)}{|q| + E_m - (E_M + E_D)/2}. \tag{6}$$

To make the NME dimensionless, $R = 1.2 \times A^{1/3}$ fm is introduced [3]. The wave functions and energies of odd-odd intermediate nuclear states are denoted respectively by $|m\rangle$ and E_m.

To simplify the calculations, the closure approximation is usually adopted, in which E_m is replaced by an average one $\bar{E}$ [3,49]. In such a way, using the relation $\sum_m |m\rangle\langle m| = 1$, the decay operator becomes

$$\hat{\mathcal{O}}^{0\nu} = \frac{4\pi R}{g_A^2(0)}\iint d^3x_1 d^3x_2 \int \frac{d^3q}{(2\pi)^3}\frac{e^{iq\cdot(x_1-x_2)}}{|q|}\frac{\mathcal{J}_\mu^\dagger(x_1)\mathcal{J}^{\mu\dagger}(x_2)}{|q| + E_d}, \tag{7}$$

where $E_d = \bar{E} - (E_M + E_D)/2$ represents the average energy. The empirical value $E_d = 1.12 \times A^{1/2}$ is used in the present calculations [13].

In the TPSM calculations, it is necessary to reduce the decay operator in Eq. (7) to the nonrelativistic form. By neglecting the small energy transferred between nucleons in the nonrelativistic expansion, the hadronic current $\mathcal{J}^{\mu\dagger}$ is reduced as [15]

$$\mathcal{J}^{\mu\dagger}(x) \rightarrow \sum_{n=1}^{A} \tau_-^n[g^{\mu 0}\mathcal{J}^0(q^2) + g^{\mu k}\mathcal{J}_n^k(q^2)]\delta(x - x_n), \tag{8}$$

where x_n represents the coordinate of the nth nucleon, and $\mathcal{J}^0(q)$ and $\mathcal{J}_n(q)$ are, respectively,

$$\mathcal{J}^0(q) = g_V(q^2),$$
$$\mathcal{J}_n(q) = -g_M i\frac{\sigma_n \times q}{2m_p} + g_A(q^2)\sigma - g_P(q^2)\frac{q\sigma_n \cdot q}{2m_p}. \tag{9}$$

Substituting Eqs. (8) and (9) into Eq. (7), one can get the decay operator in the nonrelativistic form,

$$
\begin{aligned}
\hat{\mathcal{O}}^{0\nu} &= \frac{4\pi R}{g_A^2(0)} \iint d^3x_1 d^3x_2 \int \frac{d^3q}{(2\pi)^3} \frac{e^{i\boldsymbol{q}\cdot(\boldsymbol{x}_1-\boldsymbol{x}_2)}}{|\boldsymbol{q}|} \frac{\mathcal{J}_\mu^\dagger(\boldsymbol{x}_1)\mathcal{J}^{\mu\dagger}(\boldsymbol{x}_2)}{|\boldsymbol{q}| + E_d} \\
&= \frac{4\pi R}{g_A^2(0)} \iint d^3x_1 d^3x_2 \int \frac{d^3q}{(2\pi)^3} \frac{e^{i\boldsymbol{q}\cdot(\boldsymbol{x}_1-\boldsymbol{x}_2)}}{|\boldsymbol{q}|(|\boldsymbol{q}| + E_d)} \sum_{nm}[-h_F(\boldsymbol{q}^2) + h_{GT}(\boldsymbol{q}^2)\boldsymbol{\sigma}_m\cdot\boldsymbol{\sigma}_n - h_T(\boldsymbol{q}^2)S_{nm}]\tau_-^n\tau_-^m\delta(\boldsymbol{x}_1 - \boldsymbol{x}_m)\delta(\boldsymbol{x}_2 - \boldsymbol{x}_n),
\end{aligned}
$$

(10)

with

$$
S_{mn} = 3(\boldsymbol{\sigma}_n\cdot\hat{\boldsymbol{q}})(\boldsymbol{\sigma}_m\cdot\hat{\boldsymbol{q}}) - \boldsymbol{\sigma}_m\cdot\boldsymbol{\sigma}_n. \tag{11}
$$

The terms $h_F(\boldsymbol{q}^2)$, $h_{GT}(\boldsymbol{q}^2)$, and $h_T(\boldsymbol{q}^2)$ respectively correspond to Fermi (F), Gamow-Teller (GT), and Tensor (T) momentum-dependent couplings, i.e. [15],

$$
\begin{aligned}
h_F(\boldsymbol{q}^2) &= g_V^2(\boldsymbol{q}^2), \\
h_{GT}(\boldsymbol{q}^2) &= g_A^2(\boldsymbol{q}^2)\left[1 - \frac{2}{3}\frac{\boldsymbol{q}^2}{\boldsymbol{q}^2 + m_\pi^2} + \frac{1}{3}\left(\frac{\boldsymbol{q}^2}{\boldsymbol{q}^2 + m_\pi^2}\right)^2\right] + \frac{2}{3}\frac{g_M^2(\boldsymbol{q}^2)\boldsymbol{q}^2}{4m_p^2}, \\
h_T(\boldsymbol{q}^2) &= g_A^2(\boldsymbol{q}^2)\left[\frac{2}{3}\frac{\boldsymbol{q}^2}{\boldsymbol{q}^2 + m_\pi^2} - \frac{1}{3}\left(\frac{\boldsymbol{q}^2}{\boldsymbol{q}^2 + m_\pi^2}\right)^2\right] + \frac{1}{3}\frac{g_M^2(\boldsymbol{q}^2)\boldsymbol{q}^2}{4m_p^2},
\end{aligned}
$$

(12)

where m_π and m_p are pion and proton masses, respectively.

B. Nuclear wave functions

The nuclear wave functions of the mother and daughter nuclei $|\Psi_M\rangle$ and $|\Psi_D\rangle$ in Eq. (5) are obtained from the TPSM. The Hamiltonian in the TPSM is [50]

$$
\hat{H} = \hat{H}_0 - \frac{\chi}{2}\sum_\mu \hat{Q}_\mu^\dagger \hat{Q}_\mu - G_M \hat{P}^\dagger \hat{P} - G_Q \sum_\mu \hat{P}_\mu^\dagger \hat{P}_\mu, \tag{13}
$$

which includes a spherical single-particle Hamiltonian, a quadrupole-quadrupole interaction, as well as a monopole and a quadrupole pairing interaction. The intrinsic vacuum state $|\Phi_0\rangle$ is obtained by the following variational equation:

$$
\delta\langle\Phi_0|\hat{H} - \lambda_p\hat{N}_p - \lambda_n\hat{N}_n|\Phi_0\rangle = 0. \tag{14}
$$

The Lagrange multipliers λ_p and λ_n are determined respectively by the proton number Z and neutron number N.

Based on the obtained intrinsic vacuum $|\Phi_0\rangle$, the two quasiparticle states $|\Phi_\kappa\rangle$ for even-even and odd-odd nuclei can be constructed as

$$
\begin{aligned}
\text{even-even nuclei}: \quad &|\Phi_\kappa\rangle \in \{\hat{\beta}_{\nu_i}^\dagger\hat{\beta}_{\nu_j}^\dagger|\Phi_0\rangle, \hat{\beta}_{\pi_i}^\dagger\hat{\beta}_{\pi_j}^\dagger|\Phi_0\rangle\}, \\
\text{odd-odd nuclei}: \quad &|\Phi_\kappa\rangle \in \{\hat{\beta}_{\nu_i}^\dagger\hat{\beta}_{\pi_j}^\dagger|\Phi_0\rangle\},
\end{aligned}
$$

(15)

where $\hat{\beta}_\pi^\dagger$ ($\hat{\beta}_\pi$) and $\hat{\beta}_\nu^\dagger$ ($\hat{\beta}_\nu$) are respectively the quasiparticle creation (annihilation) operators for protons and neutrons. The rotational symmetry restoration for intrinsic states $|\Phi_\kappa\rangle$ is realized by the angular-momentum projection, which leads to the projected basis,

$$
\{\hat{P}_{MK}^I|\Phi_\kappa\rangle\}, \tag{16}
$$

where the three-dimensional angular-momentum projection operator [50] is

$$
\hat{P}_{MK}^I = \frac{2I+1}{8\pi^2}\int d\Omega D_{MK}^{I*}(\Omega)\hat{R}(\Omega). \tag{17}
$$

The diagonalization of the Hamiltonian in the symmetry restored projected basis leads to the Hill-Wheeler equation,

$$
\sum_{\kappa'K'}\{\langle\Phi_\kappa|\hat{H}\hat{P}_{KK'}^I|\Phi_{\kappa'}\rangle - E^I\langle\Phi_\kappa|\hat{P}_{KK'}^I|\Phi_{\kappa'}\rangle\}F_{\kappa'K'}^I = 0, \tag{18}
$$

where $\langle\Phi_\kappa|\hat{P}_{KK'}^I|\Phi_{\kappa'}\rangle$ and $\langle\Phi_\kappa|\hat{H}\hat{P}_{KK'}^I|\Phi_{\kappa'}\rangle$ are respectively the norm matrix element and the energy kernel. They can be calculated with the efficient Pfaffian algorithm [46,47]. By solving the Hill-Wheeler equation (18), one can get the eigenvalues E^I and the corresponding projected wave functions,

$$
|\Psi^I\rangle = \sum_{K\kappa} F_{\kappa K}^I \hat{P}_{MK}^I|\Phi_\kappa\rangle. \tag{19}
$$

The obtained projected wave functions are then used to calculate the NME $M^{0\nu}$ in Eq. (5).

C. Calculation of the nuclear matrix element

With the obtained projected wave functions and the decay operator, the NME $M^{0\nu}$ can be expressed as

$$
\begin{aligned}
M_\alpha^{0\nu} &= \langle\Psi_D^I|\hat{\mathcal{O}}_\alpha^{0\nu}|\Psi_M^I\rangle \\
&= \sum_{KK'}\sum_{\kappa\kappa'}\frac{2I+1}{8\pi^2}\int d\Omega D_{K'K}^{I*}(\Omega) \\
&\quad \times \langle\Phi_{\kappa'}^D|\hat{\mathcal{O}}_\alpha^{0\nu}\hat{R}(\Omega)|\Phi_\kappa^M\rangle F_{K\kappa}^I F_{K'\kappa'}^{I*},
\end{aligned}
$$

(20)

where α denotes Fermi, Gamow-Teller, or Tensor, and $\hat{P}_{M'K'}^{I\dagger}$ commutes with the decay operator $\hat{\mathcal{O}}_\alpha^{0\nu}$ and $\hat{P}_{M'K'}^{I\dagger}\hat{P}_{MK}^I = \hat{P}_{K'K}^I\delta_{MM'}$.
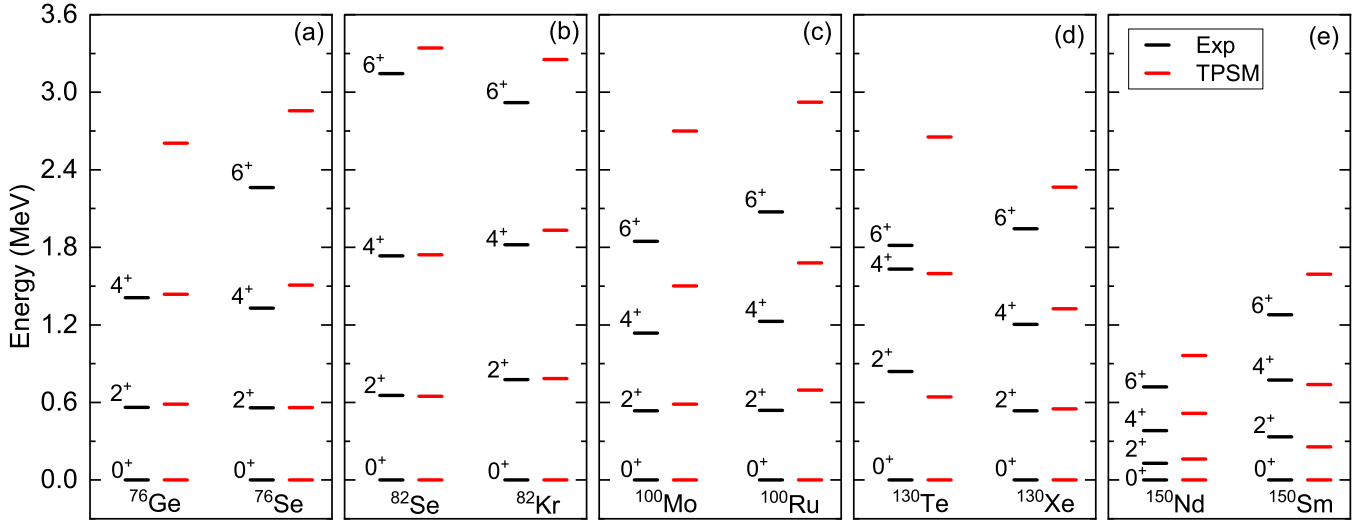
FIG. 1. Low-lying spectra for nuclei ^{76}Ge, ^{76}Se, ^{82}Se, ^{82}Kr, ^{100}Mo, ^{100}Ru, ^{130}Te, ^{130}Xe, ^{150}Nd, and ^{150}Sm calculated by the TPSM in comparison with the data [58].

The rotational matrix element $\langle \Phi^D_{\kappa'} | \hat{\mathcal{O}}^{0\nu}_\alpha \hat{R}(\Omega) | \Phi^M_\kappa \rangle$ in the second-quantized form is

$$
\begin{aligned}
\langle \Phi^D_{\kappa'} | \hat{\mathcal{O}}^{0\nu}_\alpha \hat{R}(\Omega) | \Phi^M_\kappa \rangle &= \sum_{\mu\nu\delta\gamma} \langle \mu\nu | \mathcal{O}_\alpha(1,2) | \delta\gamma \rangle \langle \Phi^D_0 | \hat{\beta}^D_b \hat{\beta}^D_a (\hat{c}^\dagger_\mu \hat{c}^\dagger_\nu)(\hat{d}_\gamma \hat{d}_\delta) \hat{R}(\Omega) \hat{\beta}^{M\dagger}_c \hat{\beta}^{M\dagger}_d | \Phi^M_0 \rangle \\
&= \sum_{\mu\nu\delta\gamma} \langle \mu\nu | \mathcal{O}_\alpha(1,2) | \delta\gamma \rangle \langle \Phi^D_0 | \hat{\beta}^D_b \hat{\beta}^D_a (\hat{c}^\dagger_\mu \hat{c}^\dagger_\nu)(\hat{d}_\gamma \hat{d}_\delta) \tilde{\hat{\beta}}^{M\dagger}_c \tilde{\hat{\beta}}^{M\dagger}_d | \tilde{\Phi}^M_0 \rangle,
\end{aligned}
\tag{21}
$$

where $\hat{c}^\dagger$ denotes the proton creation operator, $\hat{d}$ denotes the neutron annihilation operator, and $|\Phi^M_0\rangle$ and $|\Phi^D_0\rangle$ are respectively the intrinsic vacuum states of the mother and daughter nuclei. The indices μ, ν, δ, and γ run over the bases which are the eigenstates $|Nljm\rangle$ of the spherical harmonic-oscillator potential in the present paper. The detailed calculation of the two-body matrix element $\langle \mu\nu | \mathcal{O}_\alpha(1,2) | \delta\gamma \rangle$ can be found in Ref. [19].

For the evaluation of the rotational overlap $\langle \Phi^D_0 | \hat{\beta}^D_b \hat{\beta}^D_a (\hat{c}^\dagger_\mu \hat{c}^\dagger_\nu)(\hat{d}_\gamma \hat{d}_\delta) \tilde{\hat{\beta}}^{M\dagger}_c \tilde{\hat{\beta}}^{M\dagger}_d | \tilde{\Phi}^M_0 \rangle$, according to the strategy in Ref. [47], the following matrix elements of $S^{(\pm)}$ and $C^{(\pm)}$ are defined:

$$
S^{(+)}_{\mu k} =
\begin{cases}
-\dfrac{\langle \Phi^D_0 | \hat{z}_k \hat{c}^\dagger_\mu | \tilde{\Phi}^M_0 \rangle}{\langle \Phi^D_0 | \tilde{\Phi}^M_0 \rangle}, & \hat{z}_k \in \hat{\beta}^D_b, \hat{\beta}^D_a \\[3mm]
\dfrac{\langle \Phi^D_0 | \hat{c}^\dagger_\mu \hat{z}_k | \tilde{\Phi}^M_0 \rangle}{\langle \Phi^D_0 | \tilde{\Phi}^M_0 \rangle}, & \hat{z}_k \in \tilde{\hat{\beta}}^M_c, \tilde{\hat{\beta}}^M_d,
\end{cases}
\tag{22}
$$

$$
S^{(-)}_{\mu k} =
\begin{cases}
-\dfrac{\langle \Phi^D_0 | \hat{z}_k \hat{d}_\mu | \tilde{\Phi}^M_0 \rangle}{\langle \Phi^D_0 | \tilde{\Phi}^M_0 \rangle}, & \hat{z}_k \in \hat{\beta}^D_b, \hat{\beta}^D_a \\[3mm]
\dfrac{\langle \Phi^D_0 | \hat{d}_\mu \hat{z}_k | \tilde{\Phi}^M_0 \rangle}{\langle \Phi^D_0 | \tilde{\Phi}^M_0 \rangle}, & \hat{z}_k \in \tilde{\hat{\beta}}^M_c, \tilde{\hat{\beta}}^M_d,
\end{cases}
\tag{23}
$$

$$
C^{(+)}_{\mu\nu} = \frac{\langle \Phi^D_0 | \hat{c}^\dagger_\mu \hat{c}^\dagger_\nu | \tilde{\Phi}^M_0 \rangle}{\langle \Phi^D_0 | \tilde{\Phi}^M_0 \rangle}, \quad C^{(-)}_{\mu\nu} = \frac{\langle \Phi^D | \hat{d}_\mu \hat{d}_\nu | \tilde{\Phi}^M_0 \rangle}{\langle \Phi^D_0 | \tilde{\Phi}^M_0 \rangle}.
\tag{24}
$$

The rotational overlap can then be expressed as

$$
\begin{aligned}
&\langle \Phi^D_0 | \hat{\beta}^D_b \hat{\beta}^D_a (\hat{c}^\dagger_\mu \hat{c}^\dagger_\nu)(\hat{d}_\gamma \hat{d}_\delta) \tilde{\hat{\beta}}^{M\dagger}_c \tilde{\hat{\beta}}^{M\dagger}_d | \tilde{\Phi}^M_0 \rangle \\
&= C^{(+)}_{\mu\nu} C^{(-)}_{\gamma\delta} \mathrm{Pf}(X) \langle \Phi^D_0 | \tilde{\Phi}^M_0 \rangle \\
&\quad + \sum_{ij} (-1)^{i+j} \alpha_{ij} C^{(+)}_{\mu\nu} S^{(-)}_{\delta i} S^{(-)}_{\gamma j} \mathrm{Pf}(X\{i,j\}) \langle \Phi^D_0 | \tilde{\Phi}^M_0 \rangle \\
&\quad + \sum_{ij} (-1)^{i+j} \alpha_{ij} C^{(-)}_{\delta\gamma} S^{(+)}_{\mu i} S^{(+)}_{\nu j} \mathrm{Pf}(X\{i,j\}) \langle \Phi^D_0 | \tilde{\Phi}^M_0 \rangle \\
&\quad + \sum_{ijkl} \alpha_{ijkl} S^{(+)}_{\mu i} S^{(+)}_{\nu j} S^{(-)}_{\delta k} S^{(-)}_{\gamma l} \langle \Phi^D_0 | \tilde{\Phi}^M_0 \rangle,
\end{aligned}
\tag{25}
$$

where $\alpha_{ij} = 1$ for $i < j$, $\alpha_{ij} = -1$ for $i > j$, and $\alpha_{ijkl} = \alpha_{ij}\alpha_{ik}\alpha_{il}\alpha_{jk}\alpha_{jl}\alpha_{kl}$. The skew-symmetric matrix X has a dimension 4×4 and its matrix element in the lower triangle is [47]

$$
X_{ij} = \frac{\langle \Phi^D_0 | \hat{z}_i \hat{z}_j | \tilde{\Phi}^M_0 \rangle}{\langle \Phi^D_0 | \tilde{\Phi}^M_0 \rangle}, \quad i < j.
\tag{26}
$$

The $X(\{i,j\})$ in Eq. (25) represents a submatrix of X obtained by removing the rows and columns of i, j. The matrix elements $S^{(\pm)}_{\mu k}$, $C^{(\pm)}_{\mu\nu}$, and X_{ij} can be evaluated by the formulas in Ref. [47].

TABLE I. $B(E2 : 0_1^+ \rightarrow 2_1^+)$ values (in e^2 b^2) for nuclei ^{76}Ge, ^{76}Se, ^{100}Mo, ^{82}Se, ^{82}Kr, ^{100}Ru, ^{130}Te, ^{130}Xe, ^{150}Nd, and ^{150}Sm calculated by the TPSM in comparison with the data [59].

	^{76}Ge	^{76}Se	^{82}Se	^{82}Kr	^{100}Mo	^{100}Ru	^{130}Te	^{130}Xe	^{150}Nd	^{150}Sm
TPSM	0.218	0.304	0.199	0.210	0.584	0.457	0.269	0.496	3.018	2.321
Expt.	0.278	0.419	0.180	0.225	0.530	0.493	0.296	0.634	2.707	1.347

III. NUMERICAL DETAILS

In the following, the NMEs for $0\nu\beta\beta$ decay candidates ^{76}Ge, ^{82}Se, ^{100}Mo, ^{130}Te, and ^{150}Nd are calculated by the TPSM. Three harmonic-oscillator major shells around the Fermi surface are taken in the calculation for both protons and neutrons. The strengths of the monopole pairing interaction for protons and neutrons are same as those used in Ref. [30], $G_M^p = 30/A$ MeV and $G_M^n = 20/A$ MeV. Similar to Refs. [51,52], the strength of the quadrupole pairing interaction is chosen as $G_Q = 0.2G_M$. The strength of the quadrupole-quadrupole interaction χ is associated with the quadrupole deformation parameters (β, γ) by the self-consistent relation [37]. For nuclei ^{100}Mo, ^{130}Te, and ^{150}Nd as well as their daughter nuclei, the quadrupole deformation parameters (β, γ) are taken from Refs. [30,53], in which the NMEs of $0\nu\beta\beta$ decay for these three nuclei have been studied by the PHFB. For nuclei ^{76}Ge and ^{82}Se as well as their daughter nuclei ^{76}Se and ^{82}Kr, the (β, γ) values are obtained self-consistently by the calculations of the relativistic DFT [54–57].

IV. RESULTS AND DISCUSSION

The low-lying spectra for nuclei ^{76}Ge, ^{82}Se, ^{100}Mo, ^{130}Te, and ^{150}Nd as well as their daughter nuclei ^{76}Se, ^{82}Kr, ^{100}Ru, ^{130}Xe, and ^{150}Sm calculated by the TPSM are shown in Fig. 1, in comparison with the data. It is found that the level schemes are reproduced satisfactorily by the TPSM calculations, especially for the 2_1^+ states. For higher spins with $I = 4\hbar$, $6\hbar$, the calculated energy levels are slightly stretched compared with the data. The reason for the deviation might be due to the neglect of the four quasiparticle configurations in the present calculation. It is expected that the inclusion of those configurations would lower these states and work in this direction is in progress.

The $E2$ transition probabilities $B(E2 : 0_1^+ \rightarrow 2_1^+)$ calculated by the TPSM are shown in Table I, in comparison with the data [59]. The TPSM calculations reproduce the experimental $B(E2 : 0_1^+ \rightarrow 2_1^+)$ values well except for ^{150}Sm, which might be associated with a slightly large quadrupole deformation parameter β adopted in the present TPSM calculation.

The calculated occupancies of single-particle orbits for nuclei ^{76}Ge, ^{82}Se, ^{100}Mo, ^{130}Te, and ^{150}Nd as well as their
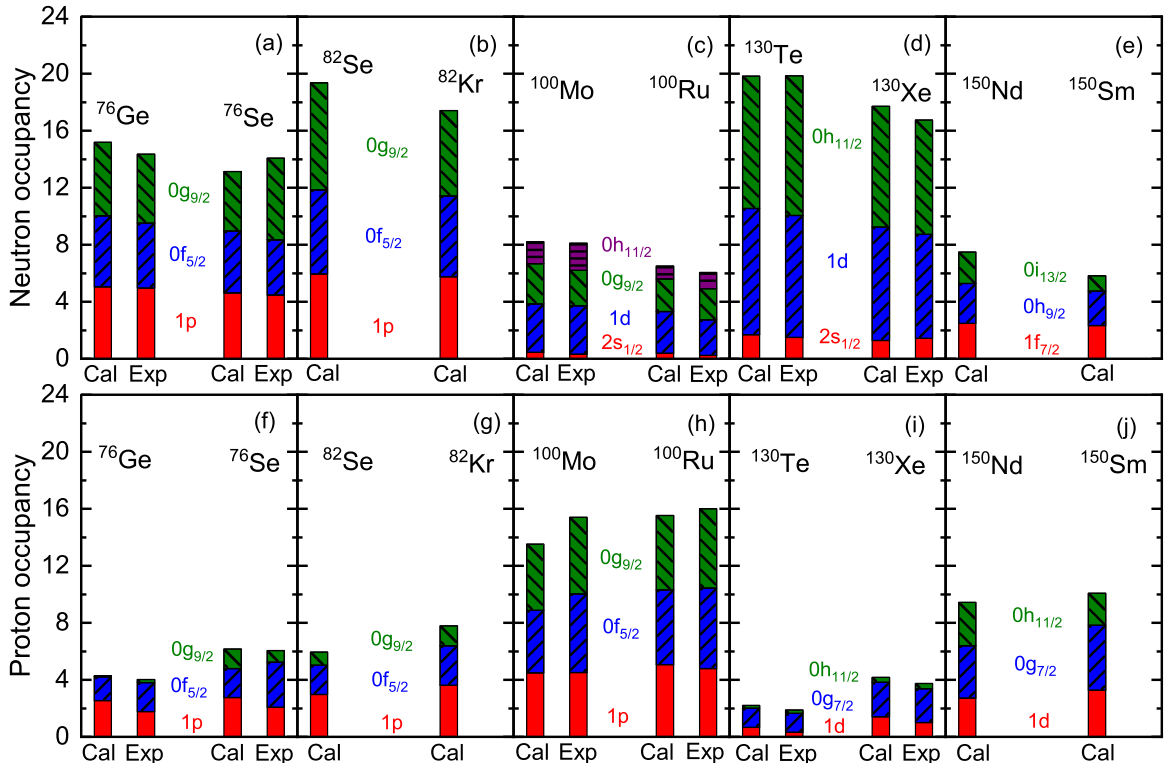

FIG. 2. The occupancies of single-particle orbits for neutrons (upper panels) and protons (lower panels) for nuclei ^{76}Ge, ^{82}Se, ^{100}Mo, ^{130}Te, and ^{150}Nd as well as their corresponding daughter nuclei, in comparison with the data available [60–64].

TABLE II. The NMEs of $0\nu\beta\beta$ decay calculated by the TPSM ($M^{0\nu}$) and TPHFB ($M^{0\nu'}$), together with their differences $\Delta M^{0\nu}$ for nuclei ^{76}Ge, ^{82}Se, ^{100}Mo, ^{130}Te, and ^{150}Nd. The contributions from Gamow-Teller ($M_{GT}^{0\nu}$, $M_{GT}^{0\nu'}$), Fermi ($M_F^{0\nu}$, $M_F^{0\nu'}$), and Tensor ($M_T^{0\nu}$, $M_T^{0\nu'}$) transitions, and the quadrupole deformation parameters (β, γ) adopted for the mother and daughter nuclei are also listed.

	(β, γ)		TPSM				TPHFB				
Decay process	Mother	Daughter	$M^{0\nu}$	$M_{GT}^{0\nu}$	$M_F^{0\nu}$	$M_T^{0\nu}$	$M^{0\nu'}$	$M_{GT}^{0\nu'}$	$M_F^{0\nu'}$	$M_T^{0\nu'}$	$\Delta M^{0\nu}$
^{76}Ge $\rightarrow$ ^{76}Se	(0.18, 0°)	(0.22, 60°)	3.17	2.67	−0.72	−0.01	3.37	2.84	−0.77	−0.01	0.20
^{82}Se $\rightarrow$ ^{82}Kr	(0.17, 0°)	(0.14, 0°)	2.59	2.16	−0.59	−0.02	2.78	2.32	−0.63	−0.02	0.19
^{100}Mo $\rightarrow$ ^{100}Ru	(0.23, 0°)	(0.21, 0°)	3.92	3.46	−0.78	−0.03	3.99	3.52	−0.79	−0.03	0.07
^{130}Te $\rightarrow$ ^{130}Xe	(0.12, 0°)	(0.17, 0°)	2.92	2.64	−0.56	−0.01	3.00	2.71	−0.58	−0.01	0.08
^{150}Nd $\rightarrow$ ^{150}Sm	(0.28, 0°)	(0.24, 0°)	3.29	2.89	−0.55	−0.02	3.44	3.02	−0.58	−0.02	0.15

corresponding daughter nuclei are shown in Fig. 2, in comparison with the data available [60–64]. The occupancies are calculated by $N_{nlj} = \sum_m \langle \Psi | \hat{N}_{nljm} | \Psi \rangle$, where $| \Psi \rangle$ is the wave function of the 0^+ state, the particle number operator is $\hat{N}_{nljm} = \hat{c}_{nljm}^{\dagger} \hat{c}_{nljm}$, and $\hat{c}_{nljm}^{\dagger}$ and $\hat{c}_{nljm}$ are the creation and annihilation operators corresponding to the spherical harmonic-oscillator basis. The calculated occupancies of spherical single-particle orbits for both neutrons and protons reproduce the data well, which add confidence to the obtained wave functions.

With the wave functions of 0^+ states obtained from the TPSM, the calculated NME $M^{0\nu}$ and the contributions from Gamow-Teller ($M_{GT}^{0\nu}$), Fermi ($M_F^{0\nu}$), and Tensor ($M_T^{0\nu}$) transitions for nuclei ^{76}Ge, ^{82}Se, ^{100}Mo, ^{130}Te, and ^{150}Nd are shown in the fourth to seventh columns of Table II. The main contribution of the NME comes from the Gamow-Teller $M_{GT}^{0\nu}$, which exhausts 85% of the total NME. The contributions of Fermi and Tensor transitions to the total NME are around 14% and 1%, respectively. Therefore, ignoring the Tensor contribution in the TPSM calculations can be a good approximation.

To study the effects of the quasiparticle configuration mixing, the NME $M^{0\nu'}$ calculated by the triaxial PHFB (TPHFB) are shown in the 8th to 11th columns in Table II. The TPHFB and the TPSM calculations are performed with the same interaction parameters in three harmonic-oscillator major shells. The difference is that the quasiparticle configuration mixing is not included in the TPHFB. The last column shows the differences $\Delta M^{0\nu}$ between $M^{0\nu'}$ and $M^{0\nu}$, which reveals the effect of quasiparticle configuration mixing missing in the TPHFB. It is found that the quasiparticle configuration mixing reduces the NMEs ranging from 2% to 7%.

The NME $M^{0\nu}$ for nuclei ^{76}Ge, ^{82}Se, ^{100}Mo, ^{130}Te, and ^{150}Nd calculated by the TPSM are compared with those from the NDFT [36], CDFT [34], IBM [28], PHFB [30], QRPA [26], and SM [65], as shown in Fig. 3. In general, the larger $M^{0\nu}$ values are given by NDFT and CDFT, the smaller ones are given by PHFB and SM, and the other results given by TPSM, QRPA, and IBM are in between. Compared with the PHFB calculation in Ref. [30], the valence space of the TPSM is chosen as three major shells, and the contribution from quasiparticle configuration mixing beyond the HFB vacuum has been taken into account.

The NMEs shown in Table II are obtained by assuming that the nuclei under consideration are all axially deformed. It is interesting to explore the evolution of NMEs with the nuclear

triaxial deformation. In Fig. 4, the NMEs of $0\nu\beta\beta$ decay for nuclei ^{76}Ge, ^{82}Se, ^{100}Mo, ^{130}Te, and ^{150}Nd as functions of the triaxial deformation parameters for the mother (γ_M) and daughter (γ_D) nuclei are shown. For nuclei ^{82}Se and ^{130}Te, the NMEs remain roughly unchanged with the triaxial deformation parameters. For ^{82}Se, the NME varies by 17%, with the largest 3.02 at ($\gamma_M = 60°$, $\gamma_D = 60°$) and the smallest 2.59 at ($\gamma_M = 0°$, $\gamma_D = 60°$). For ^{130}Te, the NME varies by 14%, with the largest 3.00 at ($\gamma_M = 0°$, $\gamma_D = 0°$) and the smallest 2.63 at ($\gamma_M = 60°$, $\gamma_D = 0°$) The insensitivity of $M^{0\nu}$ with triaxial deformation can be explained by the potential-energy curves of 0^+ states shown in Fig. 5. The potential-energy curves of 0^+ states for ^{82}Se and ^{130}Te, together with their corresponding daughter nuclei ^{82}Kr and ^{130}Xe, are rather soft, which indicates the corresponding projected wave functions are not sensitive to the triaxial deformation. This explains the nearly unchanged NMEs for ^{82}Se and ^{130}Te with γ_M and γ_D.

For nuclei ^{100}Mo and ^{150}Nd, the NMEs depend sensitively on the triaxial deformation parameters. The mother and daughter nuclei with similar triaxial deformation parameters trend to give larger $M^{0\nu}$. For ^{100}Mo, the NME varies by 68%, with the largest 4.46 at ($\gamma_M = 40°$, $\gamma_D = 60°$) and the smallest 2.65 at ($\gamma_M = 60°$, $\gamma_D = 0°$). For ^{150}Nd, the NME varies
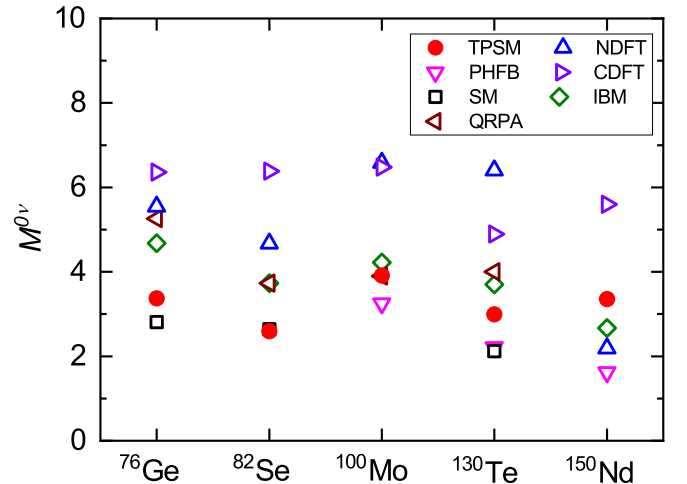

FIG. 3. The NMEs of $0\nu\beta\beta$ decay calculated by the TPSM in comparison with those from the nonrelativistic DFT (NDFT) [36], relativistic DFT (CDFT) [34], IBM [28], PHFB [30], QRPA [26], and SM [65].
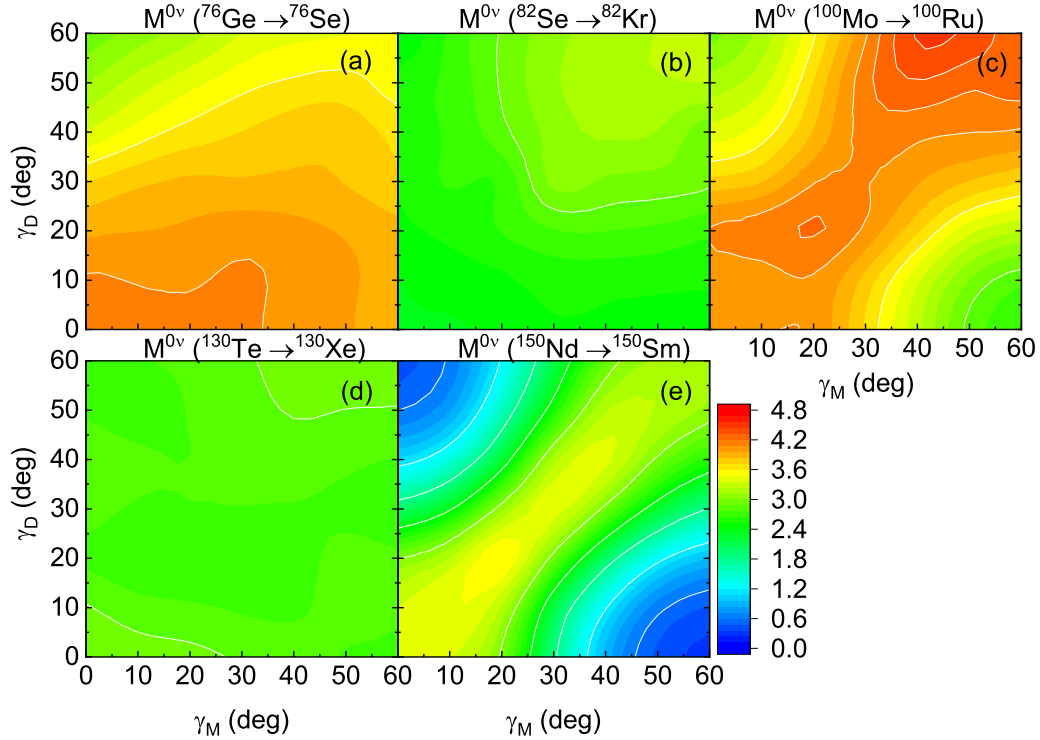
FIG. 4. The NMEs of $0\nu\beta\beta$ decay for nuclei ^{76}Ge, ^{82}Se, ^{100}Mo, ^{130}Te, and ^{150}Nd as functions of the triaxial deformation parameters for the mother and daughter nuclei.

by 511%, with the largest 3.61 at ($\gamma_M = 20°$, $\gamma_D = 20°$) and the smallest 0.59 at ($\gamma_M = 60°$, $\gamma_D = 0°$). The sensitivity of $M^{0\nu}$ with γ_M and γ_D can be explained by the stiffness of the potential-energy curves for ^{100}Mo and ^{150}Nd, together with their corresponding daughter nuclei ^{100}Ru and ^{150}Sm, as shown in Fig. 5.

Although ^{76}Ge and ^{76}Se are axially deformed in the relativistic DFT calculations, the rotational symmetry restored states 0^+ in the TPSM for ^{76}Ge and ^{76}Se are triaxially deformed with $\gamma_M = 30°$ and $\gamma_D = 40°$, as shown in Fig. 5. With these corresponding triaxial deformation parameters, the resulting $M^{0\nu}$ is 3.72 which is 17% larger than the value 3.17

in the axial deformation case shown in Table II. This indicates the importance of treating the triaxial deformation correctly when calculating the NMEs of $0\nu\beta\beta$ decay.

To simplify the calculations, the closure approximation is usually adopted except in QRPA and some SM calculations. The present TPSM treats the even-even and odd-odd nuclei in a unified way. We can investigate the effects of the closure approximation and study the contributions of odd-odd intermediate states to the NMEs. In Fig. 6, the NME $M^{0\nu}$ calculated by the TPSM with contributions of odd-odd intermediate states at different spin for nuclei ^{76}Ge, ^{82}Se, ^{100}Mo, ^{130}Te, and ^{150}Nd are shown, in comparison with the
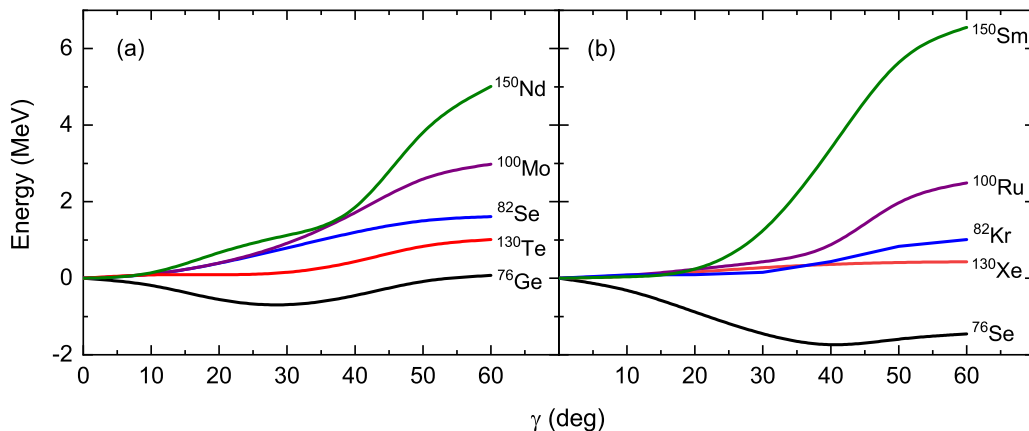

FIG. 5. Potential-energy curves of 0^+ states as functions of the triaxial deformation parameters γ for nuclei (a) ^{76}Ge, ^{82}Se, ^{100}Mo, ^{130}Te, and ^{150}Nd as well as (b) their corresponding daughter nuclei in the TPSM.
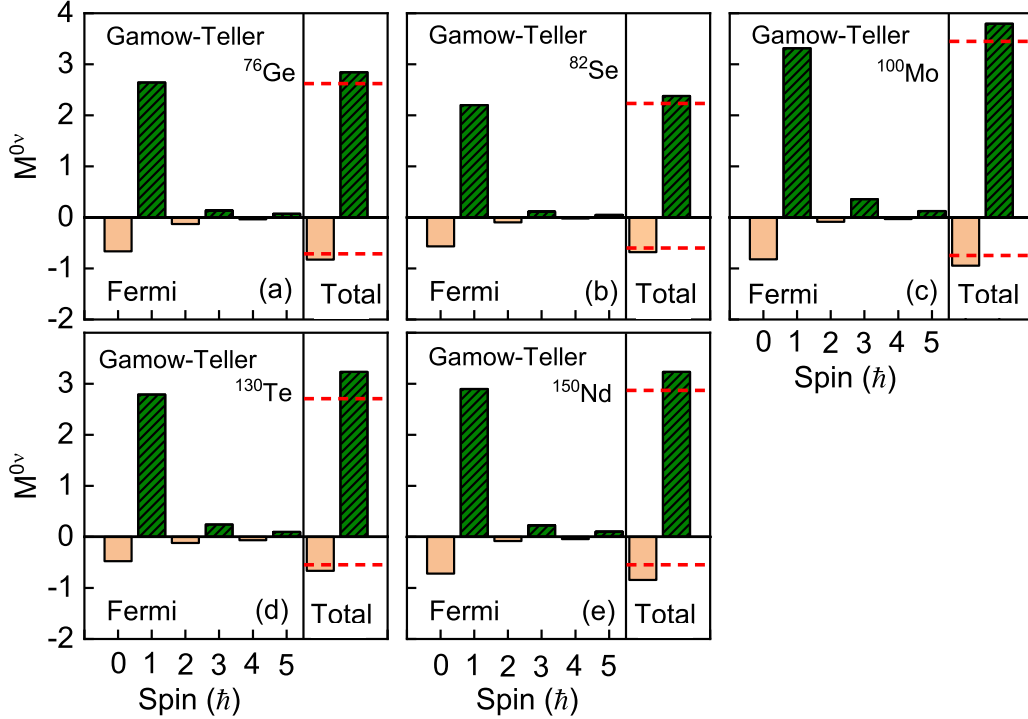
FIG. 6. The NMEs of $0\nu\beta\beta$ decay for nuclei ^{76}Ge, ^{82}Se, ^{100}Mo, ^{130}Te, and ^{150}Nd calculated by the TPSM with odd-odd intermediate states at different spin. The left panel in each subfigure denotes the contribution of the Gamow-Teller and Fermi transitions. The right panels denote the total Gamow-Teller and Fermi NMEs in comparison with the corresponding ones calculated by the closure approximation (dashed line).

results from the closure approximation. The cutoff energy for the nonclosure calculations is 6.5 MeV. The NMEs vary less than 1% with cutoff energies 7.0 and 6.5 MeV. The Gamow-Teller and the Fermi NMEs for the intermediate states at different spin are denoted by bars, and the dashed lines represent the results calculated by the closure approximation. The Gamow-Teller NMEs are mainly contributed from the odd-odd intermediate states with $I = 1\hbar$, which exhausts more than 80% of the total Gamow-Teller NMEs. This can be understood by the Gamow-Teller operator $\sigma\tau_-$ and the initial and finial states 0^+ for the mother and daughter nuclei. The Fermi NMEs are mainly contributed from the intermediate states with $I = 0\hbar$. The states with $I = 2\hbar$, $4\hbar$ contribute less than 10% to the total Fermi NMEs.

Comparing with the results in Table II with the closure approximation, the explicit calculations of the transitions through the odd-odd intermediate states enhance the NMEs. For nuclei ^{76}Ge, ^{82}Se, ^{100}Mo, ^{130}Te, and ^{150}Nd, the contribution of the odd-odd intermediate states increase respectively the values of the NMEs by 7%, 4%, 11%, 20%, and 14%, respectively. In comparison, an enhancement about 10% is given by the SM calculations for ^{48}Ca [66].

V. SUMMARY

In summary, the nuclear matrix elements of neutrinoless double-β decay for nuclei ^{76}Ge, ^{82}Se, ^{100}Mo, ^{130}Te, and ^{150}Nd are studied within the triaxial projected shell model, which incorporates simultaneously the triaxial deformation and quasiparticle configuration mixing. The low-lying spec-

tra, the $B(E2 : 0^+ \rightarrow 2^+)$ values, and the occupancies of single-particle orbits for nuclei under consideration are reproduced well. The effects of the quasiparticles configuration mixing, the triaxial deformation, and the commonly used closure approximation are examined.

The inclusion of the quasiparticle configuration mixing in the configuration space reduces the nuclear matrix element ranging from 2% to 7%. In comparison with the results by the closure approximation, the explicit calculation of the transitions through the odd-odd intermediate states systematically enhance the nuclear matrix elements for nuclei ^{76}Ge, ^{82}Se, ^{100}Mo, ^{130}Te, and ^{150}Nd by 7%, 4%, 11%, 20%, and 14%, respectively.

The mother and daughter nuclei with similar triaxial shape tend to give larger nuclear matrix elements. After examining the nuclear matrix elements as functions of the triaxial deformation parameters, it is found the nuclear matrix elements for ^{76}Ge, ^{82}Se, ^{100}Mo, ^{130}Te, and ^{150}Nd vary with γ from $0°$ to $60°$ by 41%, 17%, 68%, 14%, and 511% respectively. This indicates the importance of treating the triaxial deformation consistently in calculating the nuclear matrix elements of neutrinoless double-β decay.

Although ^{76}Ge and ^{76}Se are axially deformed in the calculations of the relativistic density-functional theory, the rotational symmetry restored states 0^+ in the triaxial projected shell model for ^{76}Ge and ^{76}Se are triaxially deformed. With these corresponding triaxial deformation $\gamma = 30°$ and $40°$, the resulting nuclear matrix element is 3.72, which is 17% larger than the value 3.17 in the axial deformation case. Future work in developing the generator coordinate method is necessary to

calculate the nuclear matrix elements for ^{76}Ge by mixing the nuclear shapes.

ACKNOWLEDGMENTS

[1] J. Schechter and J. W. F. Valle, Phys. Rev. D **25**, 2951 (1982).

[2] F. T. Avignone, S. R. Elliott, and J. Engel, Rev. Mod. Phys. **80**, 481 (2008).

[3] J. Engel and J. Menéndez, Rep. Prog. Phys. **80**, 046301 (2017).

[4] M. Agostini, G. R. Araujo, A. M. Bakalyarov, M. Balata, I. Barabanov, L. Baudis, C. Bauer, E. Bellotti, S. Belogurov, A. Bettini *et al.* (GERDA Collaboration), Phys. Rev. Lett. **125**, 252502 (2020).

[5] C. E. Aalseth, N. Abgrall, E. Aguayo, S. Alvis, M. Amman, I. J. Arnquist, F. Avignone III, H. O. Back, A. S. Barabash, P. Barbeau *et al.*, Phys. Rev. Lett. **120**, 132502 (2018).

[6] D. Q. Adams, C. Alduino, K. Alfonso, F. T. Avignone, O. Azzolini, G. Bari, F. Bellini, G. Benato, M. Biassoni, A. Branca *et al.* (CUORE Collaboration), Phys. Rev. Lett. **124**, 122501 (2020).

[7] J. Albert, G. Anton, I. Badhrees, P. Barbeau, R. Bayerlein, D. Beck, V. Belov, M. Breidenbach, T. Brunner, G. Cao *et al.*, Phys. Rev. Lett. **120**, 072701 (2018).

[8] O. Azzolini, M. T. Barrera, J. W. Beeman, F. Bellini, M. Beretta, M. Biassoni, C. Brofferio, C. Bucci, L. Canonica, S. Capelli *et al.*, Phys. Rev. Lett. **120**, 232502 (2018).

[9] R. Arnold, C. Augier, A. Bakalyarov, J. Baker, A. Barabash, A. Basharina-Freshville, S. Blondel, S. Blot, M. Bongrand, V. Brudanin *et al.*, Phys. Rev. D **93**, 112008 (2016).

[10] M.-X. Xue, Y.-L. Zhang, H.-P. Peng, Z.-Z. Xu, and X.-L. Wang, Chin. Phys. C **41**, 046002 (2017).

[11] K. Ni, Y. Lai, A. Abdukerim, W. Chen, X. Chen, Y. Chen, X. Cui, Y. Fan, D. Fang, C. Fu, L. Geng, K. Giboni, F. Giuliani, L. Gu, X. Guo, K. Han, C. He, D. Huang, Y. Huang, Y. Huang, Z. Huang *et al.*, Chin. Phys. C **43**, 113001 (2019).

[12] T. Tomoda, Rep. Prog. Phys. **54**, 53 (1991).

[13] J. Kotila and F. Iachello, Phys. Rev. C **85**, 034316 (2012).

[14] J. Meng, L. S. Song, and J. M. Yao, Int. J. Mod. Phys. E **26**, 1740020 (2017).

[15] F. Šimkovic, G. Pantis, J. D. Vergados, and A. Faessler, Phys. Rev. C **60**, 055502 (1999).

[16] J. Menéndez, D. Gazit, and A. Schwenk, Phys. Rev. Lett. **107**, 062501 (2011).

[17] L.-J. Wang, J. Engel, and J. M. Yao, Phys. Rev. C **98**, 031301(R) (2018).

[18] A. Belley, C. G. Payne, S. R. Stroberg, T. Miyagi, and J. D. Holt, Phys. Rev. Lett. **126**, 042502 (2021).

[19] L. S. Song, J. M. Yao, P. Ring, and J. Meng, Phys. Rev. C **90**, 054309 (2014).

[20] E. Caurier, J. Menéndez, F. Nowacki, and A. Poves, Phys. Rev. Lett. **100**, 052503 (2008).

[21] J. Menéndez, A. Poves, E. Caurier, and F. Nowacki, Nucl. Phys. A **818**, 139 (2009).

[22] M. Horoi and B. A. Brown, Phys. Rev. Lett. **110**, 222502 (2013).

[23] A. Neacsu and M. Horoi, Phys. Rev. C **91**, 024309 (2015).

[24] F. Šimkovic, V. Rodin, A. Faessler, and P. Vogel, Phys. Rev. C **87**, 045501 (2013).

[25] D.-L. Fang, A. Faessler, and F. Simkovic, Phys. Rev. C **92**, 044301 (2015).

[26] J. Hyvärinen and J. Suhonen, Phys. Rev. C **91**, 024613 (2015).

[27] D.-L. Fang, A. Faessler, and F. Šimkovic, Phys. Rev. C **97**, 045503 (2018).

[28] J. Barea, J. Kotila, and F. Iachello, Phys. Rev. C **91**, 034304 (2015).

[29] F. F. Deppisch, L. Graf, F. Iachello, and J. Kotila, Phys. Rev. D **102**, 095016 (2020).

[30] K. Chaturvedi, R. Chandra, P. K. Rath, P. K. Raina, and J. G. Hirsch, Phys. Rev. C **78**, 054302 (2008).

[31] P. K. Rath, R. Chandra, K. Chaturvedi, P. K. Raina, and J. G. Hirsch, Phys. Rev. C **82**, 064310 (2010).

[32] P. Rath, R. Chandra, K. Chaturvedi, and P. Raina, Front. Phys. **7**, 64 (2019).

[33] J. M. Yao, L. S. Song, K. Hagino, P. Ring, and J. Meng, Phys. Rev. C **91**, 024316 (2015).

[34] L. S. Song, J. M. Yao, P. Ring, and J. Meng, Phys. Rev. C **95**, 024305 (2017).

[35] T. R. Rodríguez and G. Martínez-Pinedo, Phys. Rev. Lett. **105**, 252503 (2010).

[36] N. L. Vaquero, T. R. Rodríguez, and J. L. Egido, Phys. Rev. Lett. **111**, 142501 (2013).

[37] K. Hara and Y. Sun, Int. J. Mod. Phys. E **04**, 637 (1995).

[38] K. Hara and Y. Sun, Z. Phys. A: Hadrons Nucl. **339**, 15 (1991).

[39] Y. Sun, J.-y. Zhang, M. Guidry, and C.-L. Wu, Phys. Rev. Lett. **83**, 686 (1999).

[40] Z.-C. Gao, Y. Chen, and Y. Sun, Phys. Lett. B **634**, 195 (2006).

[41] J. A. Sheikh, G. H. Bhat, Y. Sun, G. B. Vakil, and R. Palit, Phys. Rev. C **77**, 034313 (2008).

[42] F. Q. Chen, Q. B. Chen, Y. A. Luo, J. Meng, and S. Q. Zhang, Phys. Rev. C **96**, 051303(R) (2017).

[43] F. Q. Chen, J. Meng, and S. Q. Zhang, Phys. Lett. B **785**, 211 (2018).

[44] Y. K. Wang, F. Q. Chen, P. W. Zhao, S. Q. Zhang, and J. Meng, Phys. Rev. C **99**, 054303 (2019).

[45] Y. K. Wang, F. Q. Chen, and P. W. Zhao, Phys. Lett. B **802**, 135246 (2020).

[46] G. F. Bertsch and L. M. Robledo, Phys. Rev. Lett. **108**, 042505 (2012).

[47] Q.-L. Hu, Z.-C. Gao, and Y. Chen, Phys. Lett. B **734**, 162 (2014).

[48] J. D. Walecka, in *Muon Physics*, edited by V. W. Hughes and C. S. Wu (Academic Press, New York, 1975), pp. 113–218.

[49] J. D. Vergados, H. Ejiri, and F. Šimkovic, Rep. Prog. Phys. **75**, 106301 (2012).

[50] P. Ring and P. Schuck, *The Nuclear Many-Body Problem* (Springer Science & Business Media, New York, 2004).

[51] Y. Sun, S. Wen, and D. H. Feng, Phys. Rev. Lett. **72**, 3483 (1994).

[52] Y. Sun and D. H. Feng, Phys. Rep. **264**, 375 (1996).

[53] S. Singh, R. Chandra, P. K. Rath, P. K. Raina, and J. G. Hirsch, Eur. Phys. J. A **33**, 375 (2007).

[54] P. W. Zhao, Z. P. Li, J. M. Yao, and J. Meng, Phys. Rev. C **82**, 054319 (2010).

[55] P. W. Zhao, S. Q. Zhang, and J. Meng, Phys. Rev. C **92**, 034319 (2015).

[56] Y. K. Wang, Phys. Rev. C **96**, 054324 (2017).

[57] Y. K. Wang, Phys. Rev. C **97**, 064321 (2018).

[58] NuDat 2.8, https://www.nndc.bnl.gov/nudat2/.

[59] B. Pritychenko, M. Birch, B. Singh, and M. Horoi, At. Data Nucl. Data Tables **107**, 1 (2016).

[60] J. P. Schiffer, S. J. Freeman, J. A. Clark, C. Deibel, C. R. Fitzpatrick, S. Gros, A. Heinz, D. Hirata, C. L. Jiang, B. P. Kay, A. Parikh, P. D. Parker, K. E. Rehm, A. C. C. Villari, V. Werner, and C. Wrede, Phys. Rev. Lett. **100**, 112501 (2008).

[61] B. P. Kay, J. P. Schiffer, S. J. Freeman, T. Adachi, J. A. Clark, C. M. Deibel, H. Fujita, Y. Fujita, P. Grabmayr, K. Hatanaka, D. Ishikawa, H. Matsubara, Y. Meada, H. Okamura, K. E. Rehm, Y. Sakemi, Y. Shimizu, H. Shimoda, K. Suda, Y. Tameshige, A. Tamii, and C. Wrede, Phys. Rev. C **79**, 021301(R) (2009).

[62] S. J. Freeman, D. K. Sharp, S. A. McAllister, B. P. Kay, C. M. Deibel, T. Faestermann, R. Hertenberger, A. J. Mitchell, J. P. Schiffer, S. V. Szwec, J. S. Thomas, and H.-F. Wirth, Phys. Rev. C **96**, 054325 (2017).

[63] J. P. Entwisle, B. P. Kay, A. Tamii, S. Adachi, N. Aoi, J. A. Clark, S. J. Freeman, H. Fujita, Y. Fujita, T. Furuno, T. Hashimoto, C. R. Hoffman, E. Ideguchi, T. Ito, C. Iwamoto, T. Kawabata, B. Liu, M. Miura, H. J. Ong, J. P. Schiffer, D. K. Sharp, G. Süsoy, T. Suzuki, S. V. Szwec, M. Takaki, M. Tsumura, and T. Yamamoto, Phys. Rev. C **93**, 064312 (2016).

[64] B. P. Kay, T. Bloxham, S. A. McAllister, J. A. Clark, C. M. Deibel, S. J. Freedman, S. J. Freeman, K. Han, A. M. Howard, A. J. Mitchell, P. D. Parker, J. P. Schiffer, D. K. Sharp, and J. S. Thomas, Phys. Rev. C **87**, 011302(R) (2013).

[65] M. Horoi and A. Neacsu, Phys. Rev. C **93**, 024308 (2016).

[66] R. A. Sen'kov and M. Horoi, Phys. Rev. C **88**, 064312 (2013).